JOURNAL OF GEOPHYSICAL RESEARCH, VOL. 104, NO. D3, PAGES 3511–3526, FEBRUARY 20, 1999

Chemical characterization of ambient aerosol collected during the southwest monsoon and intermonsoon seasons over the Arabian Sea: Labile-Fe(II) and other trace metals

Ronald L. Siefert,[1] Anne M. Johansen, and Michael R. Hoffmann

Environmental Engineering Science, W. M. Keck Laboratories, California Institute of Technology, Pasadena

Abstract. Atmospheric deposition of iron (Fe) to certain regions of the oceans is an important nutrient source of Fe to the biota, and the ability of the biota to uptake Fe is dependent on the speciation of the Fe. Therefore understanding the speciation of Fe in the atmosphere is critical to understanding the role of Fe as a nutrient source in surface ocean waters. Labile ferrous iron (Fe(II)) concentrations as well as total concentrations for Fe and other important trace metals, cations, and anions were determined over the Arabian Sea for two nonconsecutive months during 1995. Ambient aerosol samples were collected during the Indian Ocean intermonsoon and southwest monsoon seasons over the Arabian Sea. Sampling took place aboard the German research vessel *Meteor* in the months of May (leg M32/3; intermonsoon) and July/August (leg M32/5; southwest monsoon). Both cruise tracks followed the 65th east meridian, traveling for 30 days each (from north to south during leg M32/3 and from south to north during leg M32/5). A high-volume dichotomous virtual impactor with an aerodynamic cutoff size of 3 μm was used to collect the fine and coarse aerosol fractions for metal analysis. A low volume collector was used to collect aerosol samples for anion and cation analysis. The analysis for labile-Fe(II) was done immediately after sample collection to minimize any possible Fe redox reactions which might occur during sample storage. The analytical procedure involved filter extraction in a formate/formic acid buffered solution at *p*H 4.2 followed by colorimetric quantification of soluble Fe(II). Metals, anions, and cations were analyzed after the cruise. Total atmospheric aqueous-labile-Fe(II) concentrations during the intermonsoon were between 4.75 and <0.4 ng m^{-3}, of which most ($>80\%$) was present in the fine fraction (<3.0 μm). During the southwest monsoon, atmospheric aqueous-labile-Fe(II) concentrations were consistently below the detection limit (<0.34 to <0.089 ng m^{-3}, depending on the volume of air sampled). Air mass back trajectories (5 day, three dimensional) showed that air masses sampled during the southwest monsoon had advected over the open Indian Ocean, while air masses sampled during the intermonsoon had advected over northeast Africa, the Saudi Arabian peninsula, and southern Asia. These calculations were consistent with the results of the statistical analysis performed on the data set which showed that the variance due to crustal species during the intermonsoon samples was greater than the variance due to crustal species during the southwest monsoon. The factor scores for the crustal components were also greater when the back trajectories had advected over the nearby continental masses. Principal component analysis was also performed with the intermonsoon samples where aqueous labile Fe(II) was above the detection limit. Aqueous labile Fe(II) did not correlate well with other species indicating possible atmospheric processing of the iron during advection.

1. Introduction

A knowledge of the detailed chemical speciation of metals in atmospheric aerosols is important to understanding their role in atmospheric chemistry (cloud chemistry) and their fate in surface ocean waters after deposition. Once deposited in the ocean, metal speciation is critical to assessing the ability of marine biota to utilize atmospherically derived trace elements as micronutrients [*Hudson and Morel*, 1990, 1993; *Morel et al*., 1991; *Wells et al*., 1994, 1995]. Recent studies have found Fe to be a rate-limiting nutrient to primary phytoplankton growth in certain regions of the open ocean [*Martin and Gordon*, 1988; *Ditullio et al*., 1993; *Kolber et al*., 1994; *Martin et al*., 1994; *Price et al*., 1994]; and the speciation of Fe is critical to the rate of Fe uptake by phytoplankton. Overall, a knowledge of the speciation of trace metals in atmospheric deposition and the subsequent speciation changes upon introduction to marine waters is important to the assessment of the ability of marine biota to utilize atmospherically derived elements.

The source of metals to cloudwater is from "dry" aerosol serving as cloud condensation nuclei or by impaction processes between the dry interstitial aerosol and the cloudwater droplets. Aqueous chemistry occurring in the cloudwater in the presence of light and in a complex matrix alters the speciation

[1]Now at Chesapeake Biological Laboratory, University of Maryland Center for Environmental Science, Solomons, Maryland.

Paper number 1998JD100067.
0148-0227/99/1998JD100067$09.00

and reactivity of these metals. Several first-row transition metals are thought to play a major role in the redox cycle of sulfur and organic compounds in the troposphere, as well as controlling free radical production in clouds [*Conklin and Hoffmann*, 1988a, b; *Faust and Hoffmann*, 1986; *Graedel et al*., 1986; *Hoffmann and Jacob*, 1984; *Jacob et al*., 1989; *Jacob and Hoffmann*, 1983; *Kotronarou and Sigg*, 1993; *Martin and Hill*, 1987; *Siefert et al*., 1994; *Weschler et al*., 1986; *Xue et al*., 1991; *Zhuang et al*., 1992b; *Zuo and Hoigné*, 1992]. Both Mn and Fe can catalyze the oxidation of S(IV) by oxygen, and together they have a synergistic effect [*Berglund and Elding*, 1995; *Berglund et al*., 1993; *Conklin and Hoffmann*, 1988b; *Faust and Allen*, 1994; *Kraft and Van Eldik*, 1989; *Martin and Good*, 1991; *Martin et al*., 1991]. *Sedlak and Hoigné* [1993, 1994] have investigated the redox cycling of Fe and Cu in the presence of oxalate, and its implications on sulfur oxidation. The photoredox chemistry of Fe(III)-hydroxy and Fe(III)-oxalato complexes with the production of Fe(II) and oxidants ($OH^{\cdot}$, $HO_2^{\cdot}/O_2^{\cdot-}$) has also been studied [*Faust and Hoigné*, 1990; *Zuo and Hoigné*, 1992]. *Zuo and Hoigné* [1994] studied the photochemical decomposition of oxalic, glyoxalic, and pyruvic acid catalyzed by iron in atmospheric waters.

Modeling studies have also looked at transition metal redox chemistry in cloudwater [*Jacob et al*., 1989; *Matthijsen et al*., 1995; *Seigneur and Constantinou*, 1995]. *Jacob et al*. [1989] modeled the accumulation of pollutants observed over Bakersfield, California, and found iron to be important for the catalytic oxidation of S(IV), while *Matthijsen et al*. [1995] used a cloud model to investigate the effect of Fe and Cu on tropospheric ozone. In addition, Fe(III) has been shown to be an important reductant of Cr(VI) to Cr(III) in cloudwater [*Seigneur and Constantinou*, 1995].

Many investigators have determined the occurrence, particle-size distribution, and sources of transition metals in the atmosphere [*Galloway et al*., 1982; *Lantzy and Mackenzie*, 1979; *Nriagu and Davidson*, 1986; *Nriagu*, 1989; *Puxbaum*, 1991]. But only a few studies have investigated the speciation or reactivity of trace metals in cloudwater [*Behra and Sigg*, 1990; *Erel et al*., 1993; *Kotronarou and Sigg*, 1993; *Xue et al*., 1991] or in ambient aerosol [*Kopcewicz and Kopcewicz*, 1991, 1992; *Siefert et al*., 1994, 1996; *Spokes et al*., 1994; *Zhu et al*., 1993; *Zhuang et al*., 1992b]. Some of these studies have investigated the speciation of Fe in ambient aerosols by determining (1) the concentration of Fe(II) [*Zhu et al*., 1993; *Zhuang et al*., 1992a], (2) the concentration of soluble Fe [*Spokes et al*., 1994; *Zhu et al*., 1993], (3) the mineral form of the Fe through Mossbauer spectroscopy [*Kopcewicz and Kopcewicz*, 1991, 1992] and the photoreactivity of the iron [*Siefert et al*., 1996].

Iron, which is one of the most abundant elements in the Earth's crust, is present primarily as various Fe(II) and Fe(III) species [*Taylor and McLennan*, 1985]. Particulate Fe is transferred to the atmosphere by wind, volcanic activity, and through anthropogenic sources [*Cass and McRae*, 1983; *Gomes and Gillette*, 1993; *Seinfeld*, 1986]. Total Fe concentrations in tropospheric aerosols range from 0.6 to 4160 ng/m^3 in remote areas, 55 to 14,500 ng/m^3 in rural areas, and 21 to 32,820 ng/m^3 in urban areas [*Schroeder et al*., 1987], and cloudwater concentrations range from 0.4 to 424 μM [*Behra and Sigg*, 1990; *Fuzzi et al*., 1988; *Jacob et al*., 1985; *Munger et al*., 1983; *Waldman et al*., 1982].

Previous studies have investigated the aerosol over the Indian Ocean. *Chester et al*. [1991] studied the distributions of aerosol trace metals over the Indian Ocean. Samples were collected during the northeast monsoon period off the coast of Oman, and in the tropical southern Indian Ocean where there were no large-scale upwind continental sources. They found strong latitudinal variations in the chemical signatures of aerosols over the Indian Ocean. Savoie *et al*. [*Savoie et al*., 1987] collected aerosol samples in the northwestern Indian Ocean and found significant variations in nitrate and non-sea-salt (NSS) sulfate concentrations which were a consequence of the variation in the impact of continentally derived aerosol.

The purpose of this study was to determine the chemical composition of ambient aerosol in both the fine and coarse aerosol fractions during the intermonsoon and southwest monsoon periods over the Arabian Sea. Specific attention was given to the speciation of Fe in the ambient aerosol by conducting labile-Fe(II) measurements immediately after sample collection during the cruise. The chemical characterization of the aerosol was used to investigate sources and other factors which control both total and labile Fe concentrations. The relationship between atmospheric labile-Fe(II) and marine biological activity, which was measured concurrently during the cruise, was also investigated.

2. Methods

2.1. Aerosol Collection

Ambient aerosol samples were collected using two collector types: (1) a high-volume dichotomous virtual impactor (HVDVI) [*Solomon et al*., 1983] and (2) a low-volume collector (LVC). Two size fractions ($D_{p,50}$ = 3.0 μm) were collected with the HVDVI, which were used to analyze for total elemental composition and Fe(II). This collector was constructed out of polycarbonate with nylon screws in order to minimize trace metal contamination and had a total flow rate of 335 ± 15 L min^{-1}. The fine and coarse sample fractions were collected on two 90-mm diameter Teflon filters (Gelman Zefluor, 1 μm pore size). Two LVCs, running at a flow rate of 27 L min^{-1} each, were used to collect aerosol samples for cation and anion analysis. The LVC consisted of an inverted high-density polyethylene 2-L bottle, serving as a rain shield, inside of which was placed a Nucleopore polycarbonate filter holder loaded with a Gelman Zefluor filter (47 mm in diameter). The aerosol collectors and laboratory equipment were acid-cleaned before use by following similar procedures as outlined by *Patterson and Settle* [*Patterson and Settle*, 1976] employing ultrapure acids from Seastar Chemicals (Sidney, British Columbia, Canada) and 18.2 MΩ-cm Milli-Q UV water. The collectors were also cleaned periodically in the field by wiping the surfaces clean with KimWipes wetted with Milli-Q UV water. Filters were stored in acid-cleaned polystyrene petri dishes taped shut with Teflon tape, placed inside two plastic bags and stored in a refrigerator during the cruise. After the cruise, the filters were sent back to Caltech (via air freight) and stored in a freezer until analysis.

A sector sampling system was used to simultaneously control all of the aerosol collectors. The system was configured to allow collection of ambient aerosol samples only when the relative wind direction was ±90° off the bow during the intermonsoon cruise and ±60° off the bow during the southwest monsoon cruise. The sector sampling system was not in operation during the first 12 samples of the intermonsoon cruise, and therefore the aerosol collectors were manually controlled. This resulted in 6 of the 12 samples during this time to have collected aerosol "out of sector" (see Discussion section for

Table 1. Sequential Extraction Procedure for Measuring Labile Fractions of Ferrous Iron (Fe(II)) Collected on the Coarse and Fine HVDVI Filters

Step	Description
1	cut a 47 mm diameter piece of the 90 mm filter using a ceramic knife and a polycarbonate die
2	place filter cut in a Teflon jar
3	"wet" the filter cut by adding approximately 0.1 mL (in 0.01 mL increments) of ethanol
4	add 20 mL of formate buffer solution (pH = 4.2, $[\text{formate}]_{\text{total}}$ = 500 μM) to the jar
5	place Teflon grid on top of filter to keep it submersed, and gently swirl solution periodically
6	after 30 min, remove 5 mL aliquot and filter (using a 0.2 μm cellulose acetate syringe filter)
7	place filtered aliquot in spectrophotometric cell (5 cm path length, semi-low volume)
8	measure absorbance, ABS (background)
9	add 0.1 mL of ferrozine solution ([ferrozine] = 6.1 mM) to spectrophotometeric cell and mix
10	measure absorbance, ABS (extraction 1): $\text{Fe(II)}_{\text{aq,labile}}$
11	rinse spectrophotometer cell
12	add 0.3 mL of ferrozine solution to remaining 15 mL of solution in jar and gently swirl solution
13	after 5 min, remove 5 mL aliquot and filter (using a 0.2 μm cellulose acetate syringe filter)
14	place filtered aliquot in spectrophotometric cell
15	measure absorbance, ABS (extraction 2): $\text{Fe(II)}_{\text{FZ,5min,labile}}$
16	rinse spectrophotometer cell
17	let extraction solution stand overnight (periodically swirling solution)
18	measure absorbance, ABS (extraction 3): $\text{Fe(II)}_{\text{FZ,22h,labile}}$

further details). Usually, 24-hour-averaged aerosol samples were collected (the actual sampling duration varied depending on the ship's cruise track during the collection period).

2.2. Labile-Fe(II) Measurements Performed Immediately After Sample Collection

Several fractions of labile Fe(II), in both the fine and coarse particles collected on the two HVDVI filters, were determined by a sequential extraction procedure. These measurements were initiated immediately (within 1 hour) after sample collection in order to minimize any changes in Fe oxidation state due to possible redox reactions occurring during sample storage. Table 1 outlines the sequential extraction procedure. Three labile fractions of Fe were quantified using the procedure: (1) aqueous-labile-Fe(II) ($\text{Fe(II)}_{\text{aq,labile}}$), (2) 5-min Ferrozine-labile-Fe(II) ($\text{Fe(II)}_{\text{FZ,5min}}$), and (3) 22-hour Ferrozine-labile-Fe(II) ($\text{Fe(II)}_{\text{FZ,22h,labile}}$). Total labile iron Fe(II) ($\text{Fe(II)}_{\text{total,labile}}$) is defined as the sum of these three fractions. Fe(II) concentrations were determined colorimetrically by complexation with ferrozine [*Stookey*, 1970; *Carter*, 1971] and subsequent absorption measurements using a portable spectrophotometer (Shimadzu UV-1201).

2.3. Analysis Performed After the Cruise

Total concentrations for 31 elements (Na, Mg, Al, K, Ca, Sc, Ti, V, Cr, Mn, Fe, Ni, Cu, Zn, Ge, As, Se, Mo, Ru, Cd, Sn, Sb, Cs, Ba, La, Ce, Sm, Eu, Hf, Pb, and Th) were measured in both the coarse and fine fractions of the atmospheric aerosol (using the filters from the HVDVI). The method included a strong acid digestion of the aerosol samples, and subsequent analysis using inductively coupled plasma mass spectrometry (ICP-MS) with a Hewlett-Packard 4500 instrument. The same samples were also analyzed on a Perkin Elmer/Sciex 6000 ICP-MS for 17 elements (Na, Mg, Al, K, Ca, Ti, V, Cr, Mn, Fe, Ni, Cu, Zn, Cd, Sb, Ba, and Pb) for quality control. Table 2 outlines the strong acid digestion technique. Indium and Bismuth were used as internal standards. Analysis of multiple isotopes was done for Mg (isotopes 24, 25, 26), Ca (isotopes 43 and 44), Ti (isotopes 47 and 48), Cr (isotopes 52 and 53), Fe (isotopes 54 and 57), Ni (isotopes 60, 61, and 62), Cu (isotopes 63 and 65), Zn (isotopes 66, 67, and 68), Ge (isotopes 69, 72, and 73), Mo (isotopes 96 and 97), Sn (isotopes 117, 118, and 119), Ba (isotopes 135 and 137), Sm (isotopes 147 and 149), Eu (isotopes 151 and 153), and Hf (isotopes 177, 178, and 179). These redundant measurements were made to check for possible interference problems.

Total atmospheric aerosol concentrations of organic anions (formate, acetate, glycolate, oxalate, succinate, malonate, maleate, fumarate, citrate), inorganic anions (sulfate, nitrate, nitrite, phosphate, chloride, bromide), and cations (sodium, calcium, magnesium, ammonium) were measured using the filters

Table 2. Strong Acid Digestion Method for HVDVI

Step	Description
1	cut a piece from the 90 mm filter using a ceramic knife and a polycarbonate die
2	place filter cut in 10 mL Teflon vial
3	add 1 g concentrated HNO_3 and 1 g concentrated HF to the vial
4	place Teflon grid on top of filter to keep it submerged, and cap vial
5	place vial on shaker table and set temperature to 50°C
6	shake vial at 50°C overnight (>12 hours)
7	remove filter cut and Teflon grid from vial
8	rinse filter cut and grid with ~1 g H_2O, with rinse solution falling into vial
9	evaporate solution in vial to dryness (purging vial with N_2 gas)
10	add 0.5 g HNO_3 to vial and shake for 1/2 hour
11	add 9.5 g H_2O to vial
12	analyze solution using ICP-MS

from the LVCs. The procedure included an ion extraction method, similar to *Derrick and Moyers* [1981], followed by separation and quantification with ion chromatography. The ion chromatograph used was a Dionex BIO-LC with the capability of switching between anion and cation modes. Anions were separated and eluted with a PAX-500 anion column (Dionex) in gradient mode with a NaOH eluent, while the cations were eluted isocratically with HCl from a IonPac CS10 cation column. Although the anions data will be used in the present paper to perform the statistical analysis mentioned below, the IC data will be treated in greater detail in a separate paper.

Total suspended particulate concentrations were determined by measuring the mass of atmospheric aerosols collected on the LVC filters and knowing the volume of air sampled. The weighing procedure involved equilibrating the filters to air at 21°C and a relative humidity of 50% overnight and then weighing (these were the same conditions used to preweigh the filters). This weighing technique is similar to the one followed by *Ligocki et al*. [1993].

2.4. Error Analysis

Errors accompanying data in the table and plots are estimated by propagating the uncertainty of every parameter in the calculation that led to the final concentration. This included the volume of air sampled (10% estimated error), cutting and extracting the filter (10% estimated error), and the precision of the analytical instrument. The standard deviation for the ICP-MS is calculated about the weighted linear regression of the calibration curve. The detection limits were defined as 3 times the standard deviation of the blank (95% confidence level) divided by the slope of the calibration curve.

2.5. Statistical Analysis and Enrichment Factor Analysis

In addition to interpreting the data based on an element's enrichment compared to a crustal tracer [*Taylor and McLennan*, 1985], a multivariate statistical analysis was performed using SPSS software. In a principal component analysis the correlation matrix of the observed variables is utilized to reduce the number of those observed variables by linearly combining them into a smaller set of independent variables, called the principal components. These principal components are orthogonal to each other and can be rotated in space in order to simplify interpretation of the data set. The common type of rotation used for this type of study is varimax rotation, during which othogonality of the principal components is retained.

3. Results and Discussion

3.1. Cruise Tracks and Air Mass Back Trajectories

Four examples of 5-day air mass back trajectories (AMBTs) for both the M32/3 and M32/5 cruise legs are presented in Figure 1. AMBTs were obtained for all days for both cruise legs; however, the two AMBTs displayed for each of the cruises are representative of the meteorological conditions encountered. The cruise track for the appropriate leg is shown in Figure 1 as a solid line. Figures 1a and 1b are AMBTs for M32/3 (intermonsoon) which began in Oman and ended in the Seychelles, and Figures 1c and 1d are AMBTs for M32/5 (southwest monsoon) which began in the Seychelles and ended in Oman. Each plot traces four different AMBTs which correspond to different initial elevations (based on pressure) at the initial position. The vertical motion of each AMBT is shown in the graph at the bottom of each diagram in Figure 1. Each symbol in the diagrams represents a period of 6 hours.

During the northern part of M32/3 (intermonsoon, Figure 1a), air masses generally came from continental sources including Africa, the Middle East, and Asia, while the southern portion of the same cruise was characterized by slower moving (observe the closely spaced points) "oceanic" air masses (Figure 1b) which had not recently advected over any continental land masses.

The southwest monsoon was dominated by strong southwest winds blowing open ocean air masses toward the northeastern part of Africa. These air masses did not reach the continent before being sampled during the southern part of the cruise (Figure 1c); however, during the northern portion of the same cruise (Figure 1d), some of the higher-elevation back trajectories did advect over continental land masses, thereby possibly entraining crustal material. This pattern of persistent high-speed air current, in the form of a system of low-level jet streams in the vicinity of the western Indian Ocean during the northern summer, named the Findlater Jet [*Findlater*, 1969], also leads to major areas of upwelling in the ocean off of the coast of Somalia, which has been the subject for many areas of research.

3.2. Total Elemental Concentrations

The mass of total suspended particulates (TSP) was determined with the filters originating from the two low-volume collectors; therefore two data points per sampling interval are represented in Figure 2. Note the higher average during the southwest monsoon, when strong winds break the ocean surface, increasing the amount of sea spray droplets reaching the collector. More evidence for this statement follows below.

The x axis of this and all the plots to follow represent both a spatial and temporal scale. Both cruise tracks were almost identical but proceeded in opposite directions; on a spatial scale the left- and right-hand sides of the plots represent Oman, while the center is in proximity to the equator. Simultaneously, the left side of the plot represents the intermonsoon, while the right represents the southwest monsoon. Vertical lines in Figures 2, 3, and 6 depicts this break in the data set. Labels on the x axes are sample identifications. Table 3 lists the collection intervals and locations (taken at midpoint in time of the interval) for each aerosol sample.

Total concentrations of Na, Mg, Al, K, Ca, Sc, Ti, V, Cr, Mn, Fe, Ni, Cu, Zn, Ge, As, Se, Mo, Ru, Cd, Sn, Sb, Cs, Ba, La, Ce, Sm, Eu, Hf, Pb, and Th were determined in both the fine and coarse fractions of the ambient aerosol. Only the elements for which most of the concentrations in the samples were above detection limit are discussed further. Plots in Figure 3 represent the atmospheric concentrations in both the fine and coarse fractions of the more noteworthy elements.

A general observation from Figure 3 is that most of the metals, except for the sea-salt tracer sodium (Figure 3c), are present at much greater abundance during the intermonsoon when air masses originated over continental masses. The crustal component is typically traced by aluminium (Figure 3a) and shows that, as expected, the crustal contribution to the total aerosol loadings is highest during the intermonsoon season. Of special interest is the distribution between the fine and coarse fractions. Since crustal material suspended in the atmosphere is mechanically derived, its characteristic particle diameter is >1 μm. Because of the 3 μm cutoff of the HVDVI, we observe a considerable Al contribution in both size fractions,

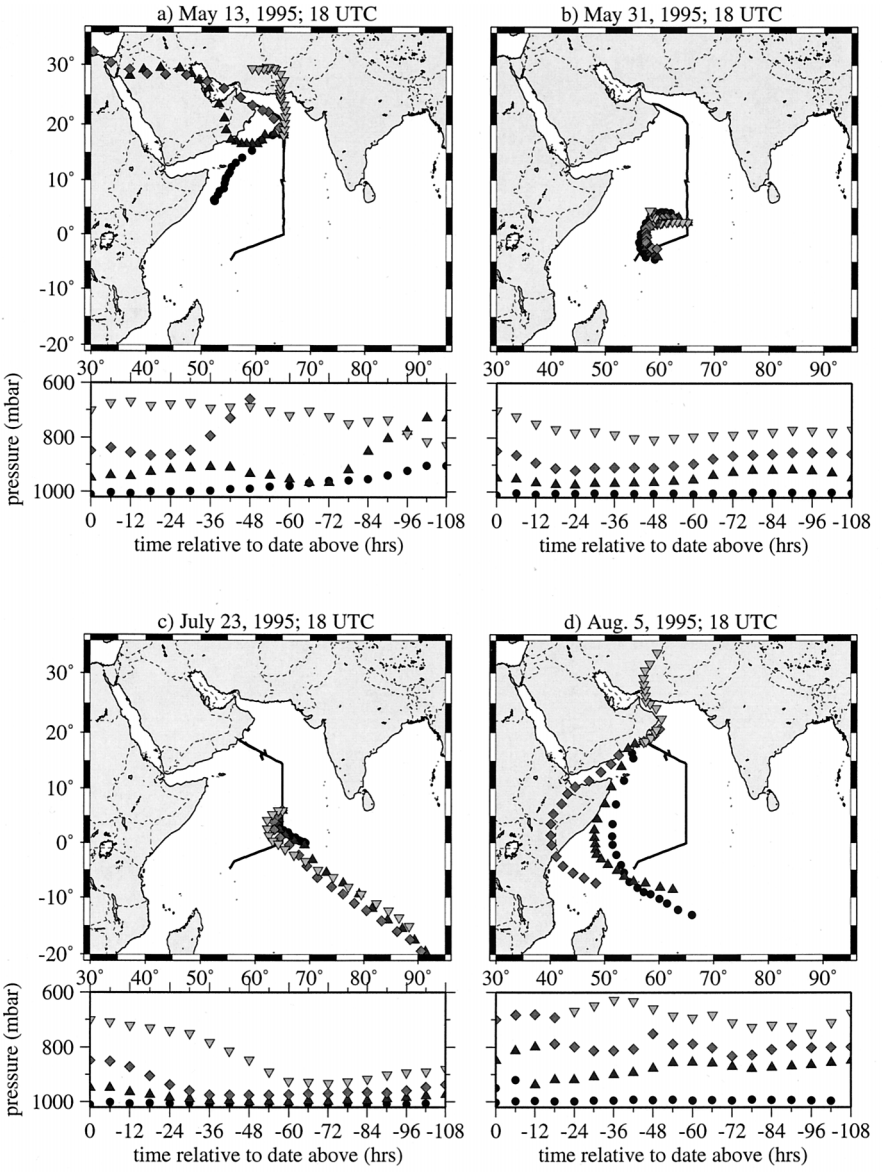

Figure 1. Five-day air mass back trajectories for four different elevations (based on pressure) above sea level for (a) May 13, 1995, 1800 UTC, (b) May 31, 1995, 1800 UTC, (c) July 23, 1995, 1800 UTC, and (d) August 5, 1995, 1800 UTC.

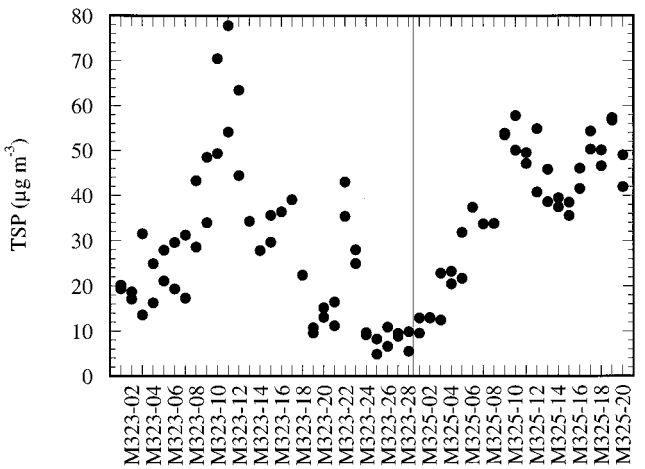

Figure 2. Total suspended particulates (TSP) over the Arabian Sea during the intermonsoon and southwest monsoon.

where the amount in the coarse fraction should dominate in closer proximity to the aerosol source. The larger the mass of a particle and the lower the wind speeds, the faster will be the removal of the aerosol from the atmosphere by dry deposition processes. This feature is well represented in Figure 3a; samples M32/3–21 through M32/3–23 (see also AMBT in Figure 1b) were taken near the equator during very low winds where air masses had traveled a substantial amount of time (>5 days) over the ocean before being sampled. The same finger print of the three fine fraction samples can be recognized in Figures 3b for Fe, 3d for Mn, 3g for Cr, and somewhat in 3e for V, indicating those elements to have a common origin. The origin of these elements will be discussed in the statistical analysis below.

Another interesting feature is the large fine contribution of lead (see Figure 3f) to its total atmospheric concentration, especially during the first half for the intermonsoon cruise. Lead is a common fuel additive still used in Africa and Asia and can therefore serve as a tracer for the anthropogenic

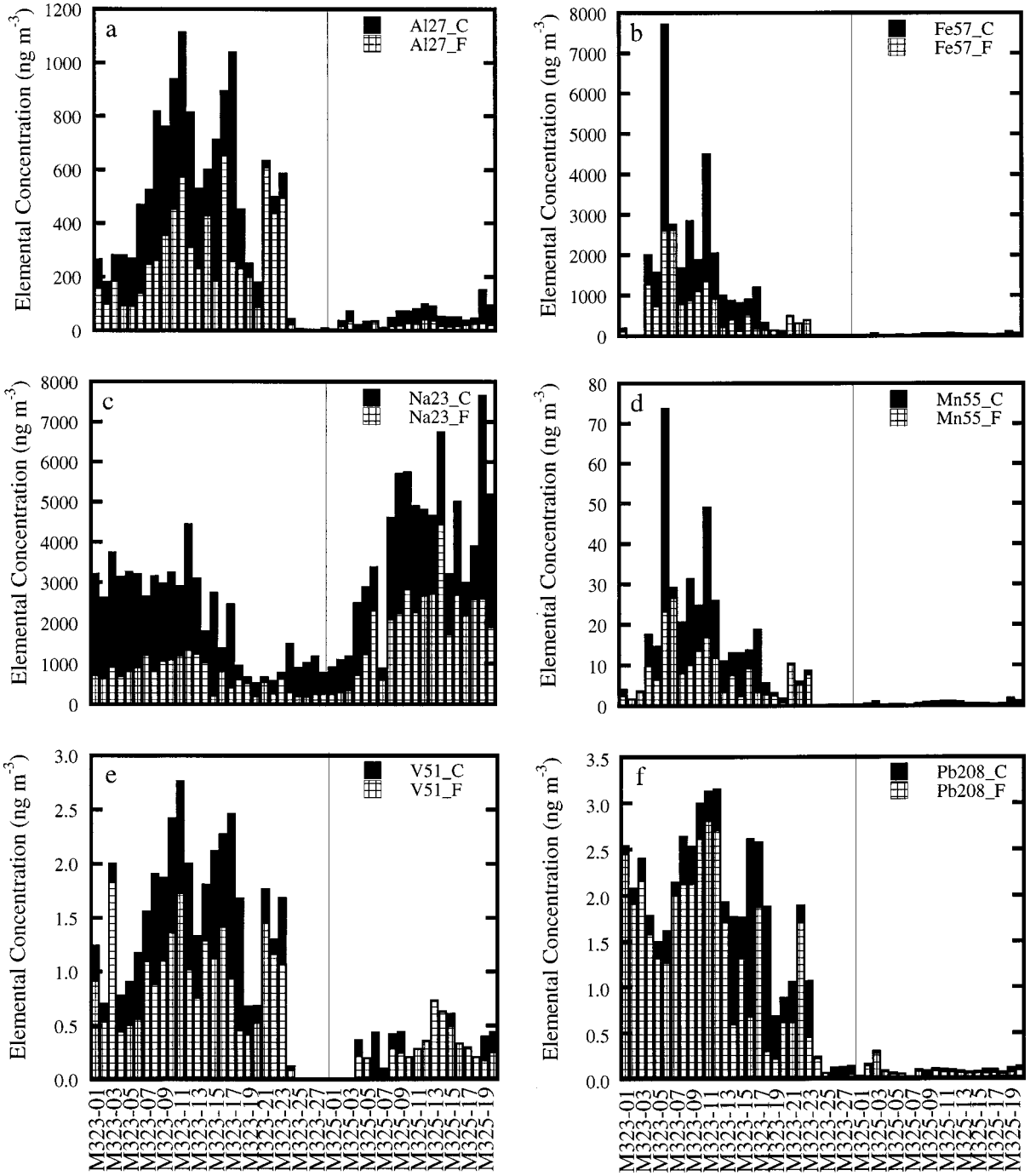

Figure 3. Concentration plots for (a) Al (m/z = 27), (b) Fe (m/z = 57), (c) Na (m/z = 23), (d) Mn (m/z = 55), (e) V (m/z = 51), (f) Pb (m/z = 208), (g) Cr (m/z = 53), (h) Mo (m/z = 95), and (i) Cu (m/z = 65). Represented are both coarse and fine fractions. Left-hand side of the dividing line indicates intermonsoon, while the right-hand side represents the southwest monsoon.

contribution of the total aerosol collected over the Arabian Sea. Because combustion processes produce submicron sized particles, we observe the enrichment of lead predominantly in the fine fraction.

Vanadium is another combustion tracer; it is inherent in crude oils and varies strongly with the region from where the oil was extracted. The heavier the oil, the higher the vanadium content. The R/V *Meteor* used diesel generators and electric engines ("diesel-electric") for its propulsion system, and diesel is a very light distillate fuel, compared with the heavy fuel oils used by most ocean-going freighters and tankers. Thus we expect most of the vanadium in the samples to be composed of an underlying crustal component plus a sporadic contribution from upwind encountered freight ships along the cruise track. The spikes in the fine V fraction observed during the southwest monsoon (the right half of Figure 3e) coincide with our steaming in the area of well defined and busy shipping lanes on the Arabian Sea.

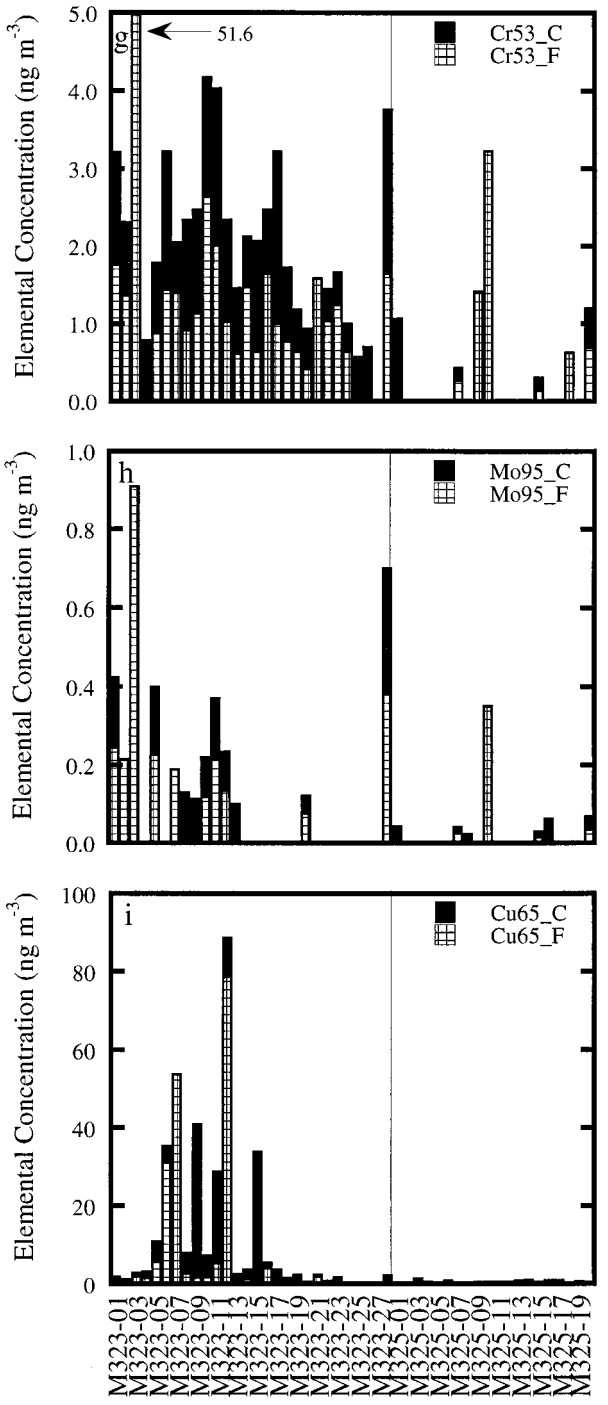

Figure 3. (continued)

3.3. Fe(II) Concentrations

Three labile fractions of Fe(II) were measured immediately after aerosol collection in both the coarse and fine aerosol fractions. Table 1 describes the sequential extraction procedure resulting in the measurements of $Fe(II)_{aq,labile}$, $Fe(II)_{FZ,5min,labile}$, and $Fe(II)_{FZ,22h,labile}$. The sum of these three labile fractions is $Fe(II)_{total,labile}$. In the discussion we will focus on the $Fe(II)_{aq,labile}$ and $Fe(II)_{total,labile}$ for both aerosol size fractions. These fractions were selected since they best represent the minimum ($Fe(II)_{aq,labile}$) and maximum ($Fe(II)_{total,labile}$) amount of Fe(II) which would be expected to be dissolved into the aqueous phase upon activation of the aerosol into cloud drops (excluding reductive dissolution processes). Only labile Fe(II) results from the intermonsoon (M32/3) are available since all the extractions during the southwest monsoon were below detection limit. The results are presented in Figures 4 and 5. Two samples are missing at either end of the cruise: at the beginning, due to the development of the extraction procedure, and at the end, due to the early disassembly of the laboratory equipment in preparation for disembarkation.

Concentrations of Fe(II) in both the fine and coarse fractions are presented in the stacked bar plots in Figure 4. The measurement for $Fe(II)_{FZ,22h,labile}$ was started using sample M323-08 for the fine fraction and M323-13 for the coarse fraction, due to the development of the labile Fe(II) extraction method during the first part of intermonsoon cruise. Therefore both the fine $Fe(II)_{total,labile}$ and the coarse $Fe(II)_{total,labile}$ are potentially biased low during the first 7 and 12 samples, respectively.

From Figure 4 we see that overall more than 80% of the $Fe(II)_{total,labile}$ was present in the fine fraction. These observations may indicate the presence of two different sources and/or a different weathering history of the two aerosol size fractions. Iron in the coarse size fraction is probably associated with crustal material, and this Fe is expected to be bound in alumino-silicate minerals, which would not be susceptible to chemical weathering on the timescale of atmospheric aerosols. However, some fraction of the crustal material may also include clay materials and iron oxides which would be more susceptible to chemical weathering and the release of Fe(II). Aerosol in the fine fraction is usually composed of secondary aerosol and primary aerosol from pollution sources; however, due to the 3 μm cutoff size in the HVDVI, we are also probably collecting crustal elements in the fine fraction. Overall, a greater fraction of the iron in the fine fraction is probably from pollution sources (e.g., combustion of fossil fuels) than in the coarse fraction, and the pollution sources may produce more labile forms of Fe such as iron oxyhydroxides. Smaller particles can also be suspended in the atmosphere much longer [*Arimoto and Duce*, 1986; *Rojas et al*., 1993] than larger particles, allowing them to undergo chemical transformation when subjected to repeated "wet" and "dry" cycles. This cycling could also result in an increase in labile Fe(II) to total Fe.

Figure 5 represents the percentages of $Fe(II)_{total,labile}$ to total Fe (determined by ICP-MS) for the fine and coarse size fractions as well as for the total (the bars represent calculated ranges based on the detection limits of the measurements). Overall, never more than 4% of the total Fe is released as Fe(II) after 22 hours of extraction. However, a greater percentage of $Fe(II)_{total,labile}$ to total Fe is observed in the fine aerosol fraction for almost all of the samples. *Zhu et al*. [1993] observed $Fe(II)_{labile}/Fe_{total}$ fractions in four Barbados aerosol samples of 0.87, 0.92, 0.47, and 0.53% which were similar to our observations. *Zhuang et al*. [1992b] observed higher $Fe(II)_{labile}/Fe_{total}$ fractions: 2.2 to 49% in marine aerosol samples collected over the central North Pacific and Barbados (see *Zhu et al*. [1993] for a correction of *Zhuang et al*. [1992b] results). These higher fractions, compared to our observations on the Arabian Sea, may be the result of increased cloud processing of the aerosol in the central North Pacific and Barbados. However, in the studies by both *Zhu et al*. [1993] and *Zhuang et al*. [1992b] the time between the collection and analysis was considerable, possibly enough to change oxidation states; whereas, in this study, analysis was performed immediately (within 1

Table 3. Aerosol Sample Collection Times and Positions

Label	Start Date/Time, UTC	Stop Date/Time, UTC	Latitude °North	Longitude °East
M32/3_01	May 9, 1995 0916	May 9, 1995 1726	16.3	65.0
M32/3_02	May 9, 1995 1750	May 10, 1995 0415	16.7	65.0
M32/3_03	May 10, 1995 0640	May 10, 1995 1200	18.0	65.0
M32/3_04	May 10, 1995 1300	May 11, 1995 0221	18.0	65.0
M32/3_05	May 11, 1995 0240	May 11, 1995 0715	18.0	65.0
M32/3_06	May 11, 1995 1410	May 11, 1995 2330	18.1	65.0
M32/3_07	May 12, 1995 0415	May 12, 1995 2230	18.1	65.0
M32/3_08	May 13, 1995 0430	May 13, 1995 2200	18.1	65.0
M32/3_09	May 14, 1995 0310	May 14, 1995 2215	18.1	65.0
M32/3_10	May 15, 1995 0320	May 15, 1995 2230	18.1	65.0
M32/3_11	May 16, 1995 0315	May 16, 1995 1655	18.1	65.0
M32/3_12	May 17, 1995 0321	May 18, 1995 0310	18.1	65.0
M32/3_13	May 18, 1995 0335	May 19, 1995 0305	16.9	65.0
M32/3_14	May 19, 1995 0320	May 20, 1995 0315	14.3	65.0
M32/3_15	May 20, 1995 0335	May 21, 1995 0310	11.5	65.0
M32/3_16	May 21, 1995 0335	May 22, 1995 0310	10.0	65.0
M32/3_17	May 22, 1995 0320	May 23, 1995 0315	10.0	65.0
M32/3_18	May 23, 1995 0330	May 24, 1995 0315	10.0	65.0
M32/3_19	May 24, 1995 0325	May 25, 1995 0315	10.0	65.0
M32/3_20	May 25, 1995 0330	May 26, 1995 0325	10.0	65.0
M32/3_21	May 26, 1995 0335	May 27, 1995 0315	9.9	65.0
M32/3_22	May 27, 1995 0335	May 28, 1995 0320	9.5	65.0
M32/3_23	May 28, 1995 0335	May 29, 1995 0315	7.5	65.0
M32/3_24	May 29, 1995 0330	May 30, 1995 0320	4.5	65.0
M32/3_25	May 30, 1995 0400	May 30, 1995 2100	3.0	65.0
M32/3_26	May 31, 1995 0340	June 1, 1995 0300	2.9	65.0
M32/3_27	June 1, 1995 0725	June 1, 1995 2155	1.4	65.0
M32/3_28	June 2, 1995 0455	June 2, 1995 1155	0.0	65.0
M32/5_01	July 16, 1995 0910	July 17, 1995 1019	0.0	65.0
M32/5_02	July 18, 1995 0446	July 20, 1995 1025	1.5	65.0
M32/5_03	July 20, 1995 1043	July 21, 1995 0402	3.1	65.0
M32/5_04	July 21, 1995 1137	July 22, 1995 1415	6.0	65.0
M32/5_05	July 24, 1995 0102	July 25, 1995 0240	10.0	65.0
M32/5_06	July 26, 1995 0409	July 26, 1995 1315	13.0	65.0
M32/5_07	July 26, 1995 2357	July 28, 1995 1115	14.5	64.7
M32/5_08	July 28, 1995 1147	July 30, 1995 0021	15.2	63.5
M32/5_09	July 30, 1995 0033	July 31, 1995 0405	16.1	62.0
M32/5_10	July 31, 1995 0423	Aug. 1, 1995 0412	16.7	60.7
M32/5_11	Aug. 1, 1995 0430	Aug. 2, 1995 0314	17.1	59.8
M32/5_12	Aug. 2, 1995 0330	Aug. 3, 1995 0402	17.6	58.7
M32/5_13	Aug. 3, 1995 0427	Aug. 4, 1995 0515	18.4	57.5
M32/5_14	Aug. 4, 1995 0531	Aug. 5, 1995 0309	18.6	57.2
M32/5_15	Aug. 5, 1995 0322	Aug. 6, 1995 1357	18.4	57.3
M32/5_16	Aug. 6, 1995 1411	Aug. 7, 1995 1300	18.0	58.5
M32/5_17	Aug. 7, 1995 1352	Aug. 8, 1995 1009	17.4	59.6
M32/5_18	Aug. 8, 1995 1020	Aug. 9, 1995 1407	16.4	61.0
M32/5_19	Aug. 9, 1995 2329	Aug. 11, 1995 0341	16.2	61.5
M32/5_20	Aug. 11, 1995 0354	Aug. 11, 1995 2356	16.0	62.0

hour) after sample collection (which took approximately 24 hours). In addition, their extraction techniques were performed in acidic solutions.

Another interesting observation is the increase of $Fe(II)_{total,labile}$ to total Fe in the coarse fraction for samples M32/3–21 through M32/3–23 (shown as a lower limit using the detection limit for total Fe); this corresponds to the same three samples with the large fine Fe contribution seen in Figure 3b. There is no obvious explanation for these observations. Furthermore, it seems to be against common expectations; the air masses sampled had traveled over long periods of time during which the aerosol was probably subjected to considerable weathering, photoreductively increasing its relative Fe(II) content [*Faust and Hoigné*, 1990; *Zuo and Hoigné*, 1992]. Concurrently, however, the selective removal of the larger aerosol fraction, due to their faster settling velocities, results in a large decrease in the coarse aerosol loadings, while the fine fraction is not affected in the same way. Unless the coarse side of the collector collects some fraction of the fine particles which are heavily enriched in Fe(II), there seems to be a mechanism by which Fe(II) is enriched more selectively in the coarse than in the fine aerosol fraction. This could be explained by sequential cloud processing which may affect aerosols of distinct size and composition in different ways.

Although our research focused on atmospheric particulate matter, the primary focus of the cruise was the investigation of nutrient fluxes (primarily nitrogen species) in the water column and its role on biological productivity. One major observation during the cruise was an extensive bloom of the N_2-fixing Cyanobacterium, *Trichodesmium erythraeum* [*Capone et al.*, 1998]. In addition, the ability of Trichodesmium erythraeum to sequester new nitrogen makes it an important component of biological productivity in the central Arabian Sea, which is oligotrophic. The enzyme, which is responsible for nitrogen

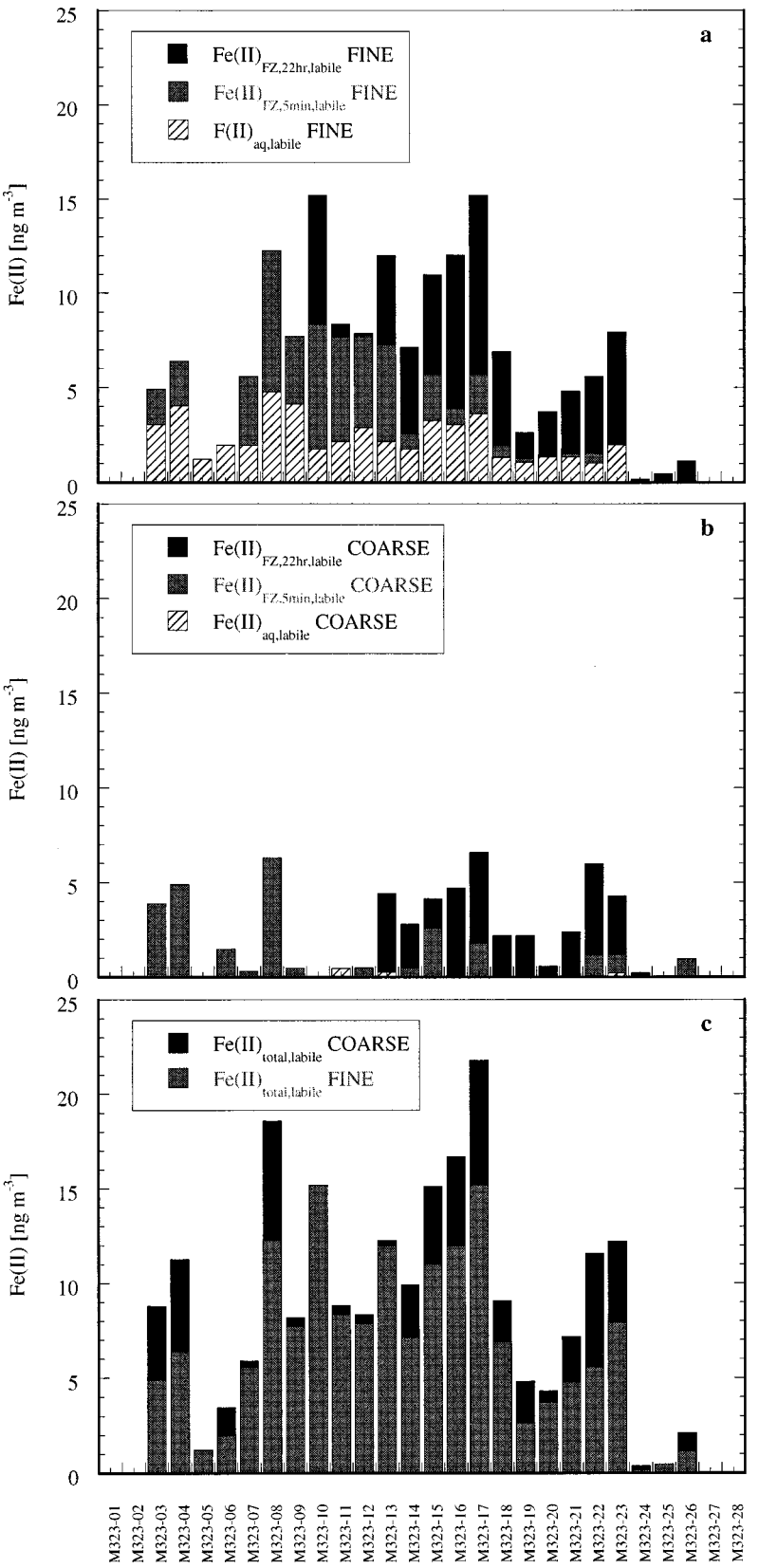

Figure 4. Labile-Fe(II) concentrations for the (a) fine, (b) coarse, and (c) total aerosol fractions during the intermonsoon (no data for the southwest monsoon are presented since all the measurements were below the detection limit).

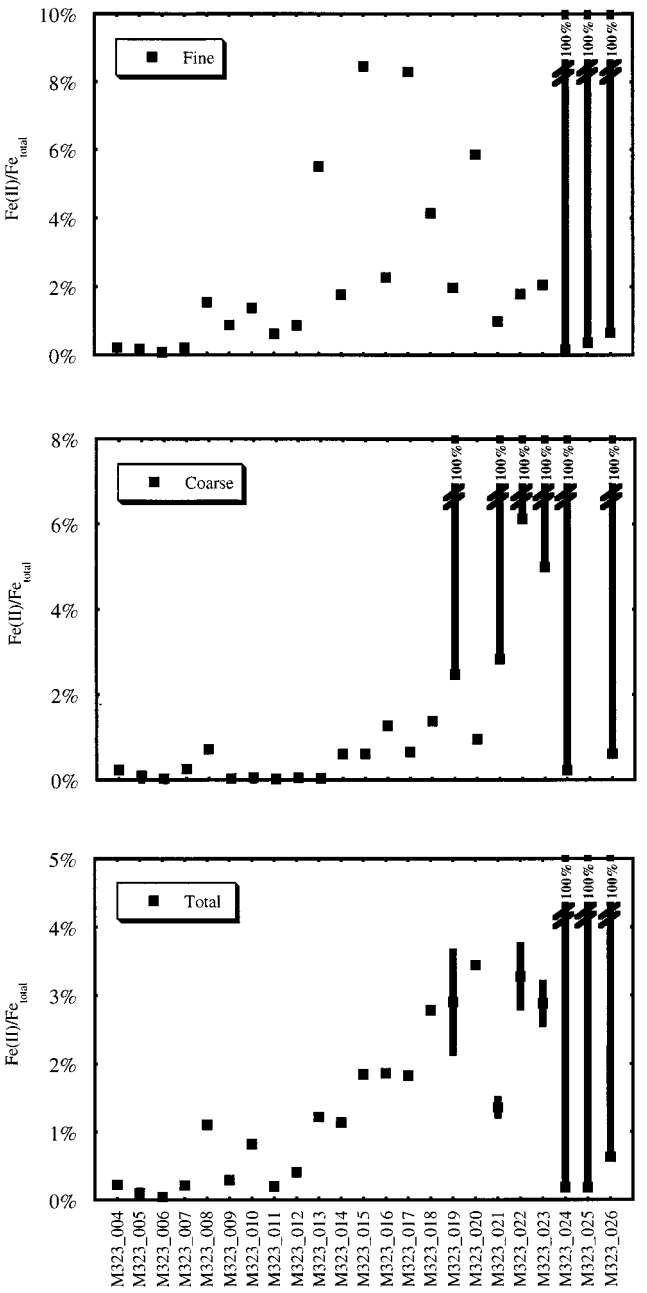

Figure 5. Percentage of $Fe(II)_{total,labile}$ to Fe_{total} for the fine, coarse, and total aerosol fractions during the intermonsoon (no data for the southwest monsoon are presented since all the measurements were below the detection limit.

fixation in *Trichodesmium erythraeum*, has relatively large amounts of Fe in its chemical structure. Therefore correlations between atmospheric labile-Fe(II) and *Trichodesmium erythraeum* were investigated (for more details, see *Capone et al.* [1998]). We observed a correlation between labile-Fe(II) and *Trichodesmium erythraeum*; however, the evidence is not conclusive.

3.4. Enrichment Factors

Enrichment factors (EF) were determined [*Zoller et al.*, 1974; *Duce et al.*, 1975] for a series of elements using their total (fine plus coarse fractions) atmospheric concentrations. Crustal averages from *Taylor and McLennan* [1985] were used as a reference using Al as the crustal tracer. The values are listed in Table 4. The closer the value is to 1, the stronger the indication is that a specific element in the sample was associated with the crustal component of the aerosol.

Iron seems to be predominantly of crustal origin during the southwest monsoon (M325), while during the intermonsoon (M323), over a third of the samples are enriched (>2), suggesting another source of Fe, especially in the first half of that cruise. EFs for Mn reveal the same relative enrichment pattern as Fe, however, at lower values. This resemblance is clearly visible when comparing the Fe and Mn plots in Figure 3b and 3d, respectively. Cr, Cu, Zn, Mo, and Sn are also elements which are enriched above normal when Fe and Mn are enriched. Although the reason for these enrichments is not clear, two speculated sources of these enrichments may be contamination (e.g., ship exhaust) or a natural source of these elements. One potential natural source which may explain the enrichment observations is ultramafic rock which has an elemental profile which is generally consistent with the observed enrichments. Ultramafic rock is made up of ferromagnesian minerals (olivine and pyroxene), which, as the name suggests, contain higher than normal concentrations of iron and manganese. These types of rocks are associated with the Earth's mantle, of which a piece, known as the Samail ophiolite formation [*Hess*, 1989], is residing on the coast of Oman. Table 5 lists the composition of a typical ultramafic rock and that of the crustal average used in determining the above enrichment factors. In order to directly compare the EFs in Table 4 with the elemental content of the ultramafic rock, the elemental concentrations of the ultramafic rock were normalized with regard to the crustal average in the same manner as the EF were determined. Thus the third column denotes the enrichment of a typical ultramafic rock over the crustal average. Assuming all the aerosol in a sample was made up of this ultramafic rock, one should observe the maximum EF for an element in that sample (Table 4) to match the value in column 3 in Table 5. The elements in parentheses in Table 5 are the highly enriched ones; Mn, Fe, Cr, and Ni in ascending order. The observed Fe and Mn enrichments during the intermonsoon are roughly consistent with ultramafic rock; however, the observed Cr enrichments are over an order of magnitude lower than what Table 5 predicts. Overall, a natural source of the enriched Fe and Mn during the intermonsoon samples could not be identified with any strong confidence.

Vanadium enrichment during the southwest monsoon is, as mentioned in the previous section, attributable to a sporadic external source from the combustion of heavy fuel oil. Vanadium enrichment is not observed during the intermonsoon cruise; however, this does not rule out the possibility of contamination of the aerosol samples from sampling the ships exhaust since the R/V *Meteor* uses diesel which is lighter than fuel oil and therefore has much less V. The enrichment of Pb throughout all the samples indicates a steady transport of anthropogenic matter from the continents to the open ocean, where the values increase with the proximity to land masses.

Chester et al. [1991] studied the aerosol composition over the Indian Ocean during the northeast and southwest monsoons. As expected, crustal components in the aerosol loadings were small during the southwest monsoon. The wind direction during the northeast monsoon blows air from Pakistan and northern India over the Arabian Sea, thus representing different sources than the ones sampled during this study, making it difficult to compare the fingerprint of the different components.

Table 4. Enrichment Factors for a Series of Elements Based on Their Total Concentration

Sample	EF(Sc)	EF(Ti)	EF(V)	EF(Cr)	EF(Mn)	EF(Fe)	EF(Cu)	EF(Zn)	EF(Mo)	EF(Sb)	EF(Cs)	EF(Ba)	EF(La)	EF(Ce)
M323-01	1.1	1.5	1.7	5.5	0.9	0.8	8.6	21.3	134.9	200.0	6.2	1.8	2.4	2.6
M323-02	BDL	1.0	1.4	5.8	0.5	BDL	8.1	19.8	99.7	149.1	8.6	1.7	2.5	3.1
M323-03	2.9	3.9	2.6	79.4	0.8	BDL	12.3	88.3	272.7	153.2	BDL	1.6	2.2	2.5
M323-04	0.5	0.9	1.0	1.3	3.8	8.5	13.2	11.8	BDL	60.2	6.0	2.0	2.3	2.8
M323-05	0.7	1.0	1.2	3.0	3.3	7.0	46.4	8.5	125.6	147.6	6.9	2.1	2.1	2.7
M323-06	0.6	1.0	0.9	3.1	9.4	19.6	82.3	5.3	BDL	93.3	4.4	2.0	1.6	2.0
M323-07	5.2	0.9	1.1	1.8	3.3	6.3	105.9	5.9	30.3	49.4	5.7	1.9	2.5	2.7
M323-08	0.6	0.9	0.9	1.3	1.5	2.4	10.9	4.4	13.4	29.9	5.6	1.9	2.2	2.4
M323-09	0.7	1.0	0.9	1.5	2.5	4.5	58.7	5.7	12.5	39.7	5.6	1.9	2.4	2.6
M323-10	0.6	1.0	0.9	2.0	1.6	2.4	8.7	4.2	19.7	27.4	5.8	1.9	1.8	2.1
M323-11	0.6	0.9	0.9	1.6	2.6	4.8	28.8	4.0	28.0	38.2	5.5	1.8	1.7	1.9
M323-12	0.6	1.1	0.9	1.3	1.9	3.0	119.8	7.8	24.2	33.8	5.6	2.0	2.3	2.6
M323-13	0.6	1.0	0.9	1.3	1.3	2.3	5.7	4.3	16.0	29.0	5.0	2.0	1.8	2.1
M323-14	0.8	1.4	1.1	1.6	1.3	1.7	6.9	3.8	BDL	24.0	5.8	2.6	1.3	1.7
M323-15	0.7	1.1	1.1	1.3	1.1	1.4	51.8	3.3	BDL	20.9	4.8	2.1	2.5	2.7
M323-16	0.7	1.1	0.9	1.3	0.9	1.2	6.6	3.5	BDL	20.4	5.0	2.1	2.1	2.4
M323-17	0.7	1.1	0.9	1.4	1.1	1.4	4.0	3.1	BDL	23.2	4.9	2.1	2.6	2.7
M323-18	0.7	1.1	1.4	1.7	0.7	0.9	3.8	4.2	BDL	22.0	5.2	2.1	2.0	2.6
M323-19	0.9	1.1	1.0	2.2	0.8	0.6	10.1	4.6	BDL	24.6	9.0	2.2	2.1	2.5
M323-20	1.1	1.3	1.4	2.4	0.6	0.8	3.4	6.1	57.1	38.7	6.2	2.1	2.3	2.5
M323-21	1.0	1.3	1.0	1.1	1.0	0.9	3.9	2.7	BDL	13.7	12.2	2.7	1.1	1.6
M323-22	0.7	1.0	1.0	1.3	0.7	0.7	1.8	3.6	BDL	39.1	9.6	2.1	2.0	2.3
M323-23	1.1	1.1	1.1	1.3	0.9	0.8	3.2	2.9	BDL	29.8	11.4	2.3	1.1	1.7
M323-24	BDL	1.0	1.0	10.5	BDL	BDL	9.7	5.8	BDL	BDL	BDL	1.5	1.8	2.0
M323-25	BDL	BDL	BDL	BDL	BDL	BDL	BDL	BDL	BDL	BDL	BDL	BDL	BDL	BDL
M323-26	BDL	BDL	BDL	BDL	BDL	BDL	BDL	BDL	BDL	BDL	BDL	BDL	BDL	BDL
M323-27	BDL	BDL	BDL	BDL	BDL	BDL	BDL	BDL	BDL	BDL	BDL	BDL	BDL	BDL
M323-28	40.5	9.1	BDL	190.3	BDL	2.3	271.4	160.9	6567.1	BDL	BDL	2.7	5.6	8.7
M325-01	BDL	14.9	BDL	103.0	BDL	0.9	95.4	51.5	761.5	BDL	BDL	1.7	1.3	1.8
M325-02	0.6	1.1	BDL	BDL	0.8	0.9	9.2	20.5	BDL	BDL	BDL	2.0	2.1	3.0
M325-03	1.1	1.4	BDL	BDL	0.9	1.0	21.6	11.9	BDL	BDL	BDL	1.9	2.4	2.7
M325-04	1.6	1.8	6.2	BDL	0.7	1.2	28.1	39.1	BDL	BDL	BDL	2.0	3.4	49.7
M325-05	3.1	1.2	2.2	BDL	0.7	0.8	16.0	6.1	BDL	BDL	BDL	1.7	2.1	2.5
M325-06	7.5	1.1	4.5	BDL	0.5	0.9	30.6	17.8	BDL	BDL	BDL	1.5	1.9	2.0
M325-07	9.1	1.5	3.7	19.2	0.5	1.0	33.5	17.2	346.3	BDL	BDL	1.6	1.7	2.1
M325-08	1.9	1.0	3.2	BDL	0.6	0.7	13.4	5.7	41.7	BDL	BDL	1.4	1.6	2.1
M325-09	0.8	1.3	2.3	9.0	0.7	0.9	11.5	6.5	BDL	BDL	BDL	1.2	1.9	2.6
M325-10	1.9	1.0	1.1	20.7	0.8	1.0	13.0	8.4	416.1	BDL	BDL	1.2	2.3	2.4
M325-11	2.0	1.1	1.3	BDL	0.8	0.9	9.2	4.1	BDL	BDL	BDL	1.3	2.2	2.7
M325-12	1.3	1.0	1.3	BDL	0.7	0.8	9.4	5.1	BDL	BDL	BDL	1.1	2.0	2.4
M325-13	3.9	1.0	3.0	BDL	0.7	0.8	12.0	5.3	BDL	BDL	BDL	1.2	1.8	2.2
M325-14	4.1	1.2	4.4	BDL	0.7	0.8	26.0	9.5	BDL	BDL	BDL	1.2	1.9	2.4
M325-15	3.5	1.1	4.5	2.8	0.7	0.8	17.3	6.1	50.1	BDL	3.8	1.4	2.3	2.7
M325-16	13.0	1.5	2.5	BDL	0.7	0.8	25.7	12.4	107.0	BDL	BDL	1.2	1.9	2.1
M325-17	9.2	1.4	2.9	BDL	0.6	0.8	31.2	21.9	BDL	BDL	BDL	1.2	1.7	1.9
M325-18	2.1	1.3	1.7	6.3	0.7	0.9	13.9	9.5	BDL	BDL	BDL	1.3	3.2	4.2
M325-19	0.8	1.2	1.0	BDL	0.7	0.8	7.6	3.9	BDL	BDL	3.6	1.3	1.9	2.3
M325-20	1.1	1.3	1.7	5.8	0.8	0.9	10.2	5.3	60.7	BDL	4.6	1.5	2.2	2.6

Intermonsoon (M323) and southwest monsoon (M325) samples are shown. BDL, below detection limit.

3.5. Factor Analysis

Principal component analysis, also called factor analysis, serves to simplify the interpretation of a large data set by reducing the number of observed variables. The correlation matrix for the data set is used to combine those variables which correlate strongly into independent variables, resulting in a smaller set of orthogonal variables that describe the total variance of the data almost as well as the original set of variables. These new variables, called principal components or factors, usually represent the distinct sources by which the sampled aerosol is composed. This identification of different sources is essential to the knowledge of the detailed chemical composition as well as to estimating the potential for chemical transformation of the aerosol during its residence time in the atmosphere. In the presence of a contamination source which contributes significantly to the variance of the data set, a factor with those characteristics will emerge for the analysis. However, this is only the case if the source's chemical composition contributes significantly to the variance of the data set. This will be discussed in further detail below.

The first principal component analysis was performed using the measurements from both cruises. The intermonsoon and southwest monsoon measurements were combined for this analysis since the potential sources, deduced from the AMBTs, for both the cruises will be the same, due to the relatively large sampling area covered. The observed variables used in the analysis were the fine and coarse elemental compositions, the total anion and cation concentrations, and the wind speed. Only those measurements with most of the values above the detection limit were included in the analysis. Table 6 lists the result obtained from the factor analysis (employing varimax rotation), and Table 7 lists the analysis statistics for the same analysis. Missing data points (e.g., variables below the detection limit) were replaced by the average value of the detection

Table 5. Elemental Abundances in Ultramafic Rock and Crustal Average

Element (ppm Unless Otherwise Noted)	Ultramafic[a]	Crustal Average[b]	EF of Ultramafic Rock Compared to Crustal Average
Mg, %	23.2	3.2	50.8
Al, %	1.2	8.4	1.0
Si, %	19.8	26.8	5.17
K, %	0.017	0.9	0.13
Sc	10	30	2.3
Ti	300	5300	0.4
V	40	230	1.2
(Cr)	(1800)	(185)	(68.1)
(Mn)	(1560)	(1400)	(7.80)
(Fe), %	(9.64)	(7.06)	(9.56)
Co	175	29	42
(Ni)	(2000)	(105)	(133)
Cu	15	75	1.4
Zn	40	80	3.5
Sr	5.5	260	0.1
Mo	0.3	1	2.1
Sn	0.5	2.5	1.4
La	1.3	16	0.6
Ce	3.5	33	0.7
Pb	0.5	8	0.4
Th	0.0045	3.5	0.0090

[a]*Faure* [1991], *Turekian and Wedepohl* [1961], and *Vinogradov* [1962].
[b]*Taylor and McLennan* [1985].

limit for the variable. Table 6 shows all the extracted components with an eigenvalue greater than 1. The extracted components in Table 6 describe 87.3% of the total variance of the data set, of which over half (63.9.0%) is accounted for by the first three components. Figure 6 displays the factor scores for each factor plotted against the sample number. Since factor scores are the weight of each factor in a sample, the curves in Figure 6 show the relative contribution of each component in every sample in terms of variance.

The results in Table 6 are interpreted by how close the correlation coefficient is to 1. The closer a value is to 1, the better it correlates with that specific component. Several elements in one component that exhibit values close to 1 correlate with each other. To ease the reading of this table, correlation coefficients greater than 0.5 were printed in parentheses. Thus factor 1 is characterized by a coarse crustal component, due to the high correlation with coarse aluminium and the high correlation coefficients with other elements in the coarse fraction which also had enrichment factors close to 1 in Table 4 (Ba, Ce, La, Sc, and Zn). Factor 2 displays the same character as factor 1, however, for the fine fraction. The reason for these two distinct crustal components is probably due to the different removal rates of these distinct size fractions. Qualitative evidence for this can be seen by noticing the greater variation in the factor loadings for the crustal fine component (Figure 6b) toward the later part of the intermonsoon cruise, compared to the greater variation in the factor loadings for the crustal coarse component (Figure 6a) earlier during the intermonsoon cruise where the advection of the crustal aerosol from the source regions was less. These two crustal components predominate the variance during the intermonsoon, as can be seen in Figure 6 and Table 7. Factor 3 has high correlation coefficients with species associated with sea salt, including several anions (i.e., Cl^-, MSA, SO_4^{2-}) and cations (i.e., Na^+, K^+, Mg^{2+}). Factor 3 also has a high correlation coefficient with wind speed. Sea spray is produced by stronger winds, which were typical during the southwest-monsoon, and result in the larger factor scores of this component in Figure 6c.

Factor 4 (Figure 6d) contributed only 8.8% to the total variance and has high correlation coefficients for Ga, Zn, Fl^-, and NH_4^+. Factor 4 has one peak on top of an underlying decline during the beginning of the intermonsoon followed by one more peak at the end of the intermonsoon and two more at the beginning of the southwest monsoon cruise. The source of the elements in factor 4 is not known. However, the NH_4^+ trend in factor 4 is consistent with the fact that the predominant sources of ammonia to the atmosphere are terrestrial (>80%) [*Schlesinger and Hartley*, 1992] and the factor 4 loadings (Figure 6d) are higher when the AMBTs showed less advection time from terrestrial sources. Of special interest are factors 5 and 6 (Figure 6e and 6f) since they describe a major source of Fe and Mn. These factors are also more predominant during the beginning of the intermonsoon cruise. The last factor (Figure 6g) has no elements with a correlation coefficient greater than 0.5.

In the case of an additional crustal source, of ultramafic nature, as considered in the enrichment factor section, we would expect to find one component characterized by the same elements as depicted in Table 5 (Cr, Mn, Fe, and Ni), unless some elements are preferentially enriched over others during the weathering process of an ultramafic rock. Unfortunately, Cr was not used for this principal component analysis since many of the measurements were below the detection limit for the southwest monsoon, and Ni was also omitted because of the contamination problem described before. Overall, there is no clear evidence from this principal component analysis or the enrichment factor analysis of the presence of an additional ultramafic crustal source.

Contamination of the samples may be a reason for some of the components and the large enrichment factors observed for some elements. Anthropogenic sources from the continents, such as smelting operations, cannot be excluded. The potential of having sampled the *Meteor*'s exhaust plume was substantial during the 6 of the first 12 samples during the intermonsoon cruise, when the sector-sampling system was not working properly. Table 8 summarizes the sector-sampling system operation during this time including the time the aerosol samplers collected out of sector and if the ship plume passed over the collectors. Owing to the burning of relatively trace metal free diesel fuel, the direct assignment of one of the unknown factors to be representative of the diesel contribution is difficult.

Throughout the cruise, a considerable amount of different kinds of waste was incinerated. Incineration took place on a sporadic timescale and included old paints and old oil. Because of the wide range of different materials burned, the exhaust may have varied its chemical fingerprint from incident to incident, making it impossible to be detected as a single and simple component in the factor analysis. Paints used on the *Meteor* contained Zn, Ti, Pb, Cr, Ba, and Fe. Note that every one of the 11 paints used on the *Meteor* only contains one or two of these metals. The chance for having sampled some of these metals from the incinerator may exist. A slight chance of sampling the plume will always exist during the maneuvering of the ship as drifters are being put out or taken in, even though the sector-sampling system is working correctly.

Factor analysis was also performed using only the intermonsoon samples and including the $Fe(II)_{aq,labile,FINE}$ measurements. The results for this factor analysis were nearly identical

Table 6. Principal Components Extracted From Intermonsoon and Southwest Monsoon Data

	Component						
Variable	Crustal Coarse	Crustal Fine	Sea Salt	Ga Zn Fl^- NH_4^+	Fe Mn Coarse	Cu Fe Mn Fine	Other
AL27_C	(0.92)	0.28	0.00	0.04	0.17	0.14	0.03
AL27_F	0.27	(0.92)	−0.20	0.05	0.08	0.12	0.03
BA137_C	(0.94)	0.24	−0.05	0.05	0.15	0.12	0.02
BA137_F	0.17	(0.91)	−0.26	0.01	0.04	0.11	0.01
CA44_C	(0.90)	0.14	0.13	0.03	0.25	0.24	0.07
CA44_F	0.23	(0.89)	0.00	−0.11	0.13	0.04	−0.15
CE140_C	(0.94)	0.26	−0.06	0.02	−0.01	0.11	−0.02
CE140_F	0.44	(0.76)	−0.19	0.10	0.13	0.18	0.07
CU65_C	(0.57)	0.20	−0.01	−0.05	0.33	−0.13	0.49
CU65_F	0.27	0.05	0.07	0.04	0.12	(0.78)	−0.17
EU153_C	(0.94)	0.15	−0.06	0.08	0.04	0.11	0.00
EU153_F	(0.52)	(0.68)	−0.14	−0.01	0.09	0.12	0.03
FE57_C	0.41	0.14	−0.02	0.09	(0.84)	0.16	0.03
FE57_F	0.28	0.23	−0.03	0.12	(0.53)	(0.71)	−0.07
GA69_C	−0.02	−0.12	−0.12	(0.88)	0.22	−0.10	−0.03
GA69_F	−0.03	−0.14	−0.14	(0.87)	0.22	0.10	0.00
K39_C	(0.83)	0.02	0.44	0.00	0.10	0.10	−0.01
K39_F	−0.03	(0.84)	0.30	−0.08	0.02	0.14	−0.01
LA139_C	(0.94)	0.27	−0.05	0.04	−0.02	0.09	0.00
LA139_F	(0.52)	(0.74)	−0.15	0.13	0.16	0.20	0.07
MG26_C	(0.75)	0.00	(0.51)	0.14	0.20	0.16	0.10
MG26_F	0.11	(0.67)	(0.62)	−0.20	0.16	0.05	−0.01
MN55_C	(0.52)	0.14	0.00	0.07	(0.78)	0.16	0.02
MN55_F	0.30	0.45	−0.06	0.12	0.46	(0.68)	−0.02
NA23_C	0.34	−0.24	(0.73)	0.13	0.03	0.07	0.06
NA23_F	−0.19	−0.02	(0.84)	−0.26	−0.01	−0.03	0.01
PB208_C	0.32	(0.66)	−0.27	0.01	−0.07	−0.11	−0.42
PB208_F	(0.59)	0.36	0.00	0.45	0.14	0.33	0.17
SC45_C	(0.84)	0.10	−0.03	0.12	0.25	−0.07	−0.04
SC45_F	−0.03	0.31	−0.06	0.15	−0.17	(0.79)	0.18
TH232_C	(0.93)	0.27	−0.07	0.10	−0.03	0.11	−0.03
TI47_C	(0.95)	0.23	−0.05	0.01	0.12	0.10	0.03
TI47_F	0.11	(0.80)	−0.14	0.43	−0.06	0.08	0.15
V51_F	0.32	(0.76)	−0.08	0.36	0.02	0.17	0.31
ZN66_C	(0.81)	0.35	−0.15	0.11	0.19	−0.10	−0.16
ZN66_F	0.04	0.20	0.14	(0.80)	−0.13	0.14	0.26
Wind speed	−0.23	−0.21	(0.78)	−0.03	0.25	0.04	0.06
Acetate	(0.71)	0.05	−0.08	0.02	0.08	−0.21	0.49
Chloride	−0.12	−0.15	(0.94)	−0.19	−0.02	−0.10	−0.02
Fluoride	0.41	0.18	−0.04	(0.74)	−0.13	−0.08	−0.25
Formate	0.11	0.08	0.49	0.23	(0.73)	−0.04	0.10
MSA	−0.05	−0.15	(0.81)	0.04	−0.05	−0.04	0.27
Nitrate	(0.53)	(0.64)	−0.22	0.24	0.02	0.04	−0.02
Oxalate	(0.50)	0.39	(0.57)	0.24	0.13	0.13	−0.10
Sulfate	0.48	0.41	(0.66)	0.18	−0.13	0.02	0.03
Ca^{2+}	(0.65)	(0.59)	0.15	−0.02	0.13	0.10	−0.09
K^+	0.11	0.05	(0.85)	0.10	0.06	0.04	−0.09
Mg^{2+}	0.00	−0.08	(0.95)	−0.08	−0.02	0.00	−0.11
Na^+	−0.12	−0.17	(0.94)	−0.16	−0.05	−0.06	−0.07
NH_4^+	0.11	0.18	−0.05	(0.76)	0.06	0.18	−0.05

Table 7. Factor Analysis Statistics for Data Presented in Table 6

Factor	Eigenvalue	Percent of Variance	Cumulative Percent
1	14.2	28.4	28.4
2	9.4	18.8	47.2
3	8.3	16.7	63.9
4	4.4	8.8	72.7
5	3.2	6.3	79.0
6	2.9	5.8	84.8
7	1.2	2.4	87.3

to the previous factor analysis and are therefore not shown. The $Fe(II)_{aq,labile,FINE}$ had a 0.67 correlation coefficient for the "crustal coarse" component, a 0.28 correlation coefficient for the "crustal fine" component, and a 0.35 correlation coefficient for the "sea salt" component. Overall, $Fe(II)_{aq,labile,FINE}$ did not load exclusively (have a high correlation coefficient) on any of the components. The inclusion of $Fe(II)_{aq,labile,FINE}$ also did not result in a new component since it probably has a relatively low contribution to the total variance. It is also interesting that the $Fe(II)_{aq,labile,FINE}$ correlated best with the crustal iron in the coarse fraction and not the fine fraction. Overall, the re-

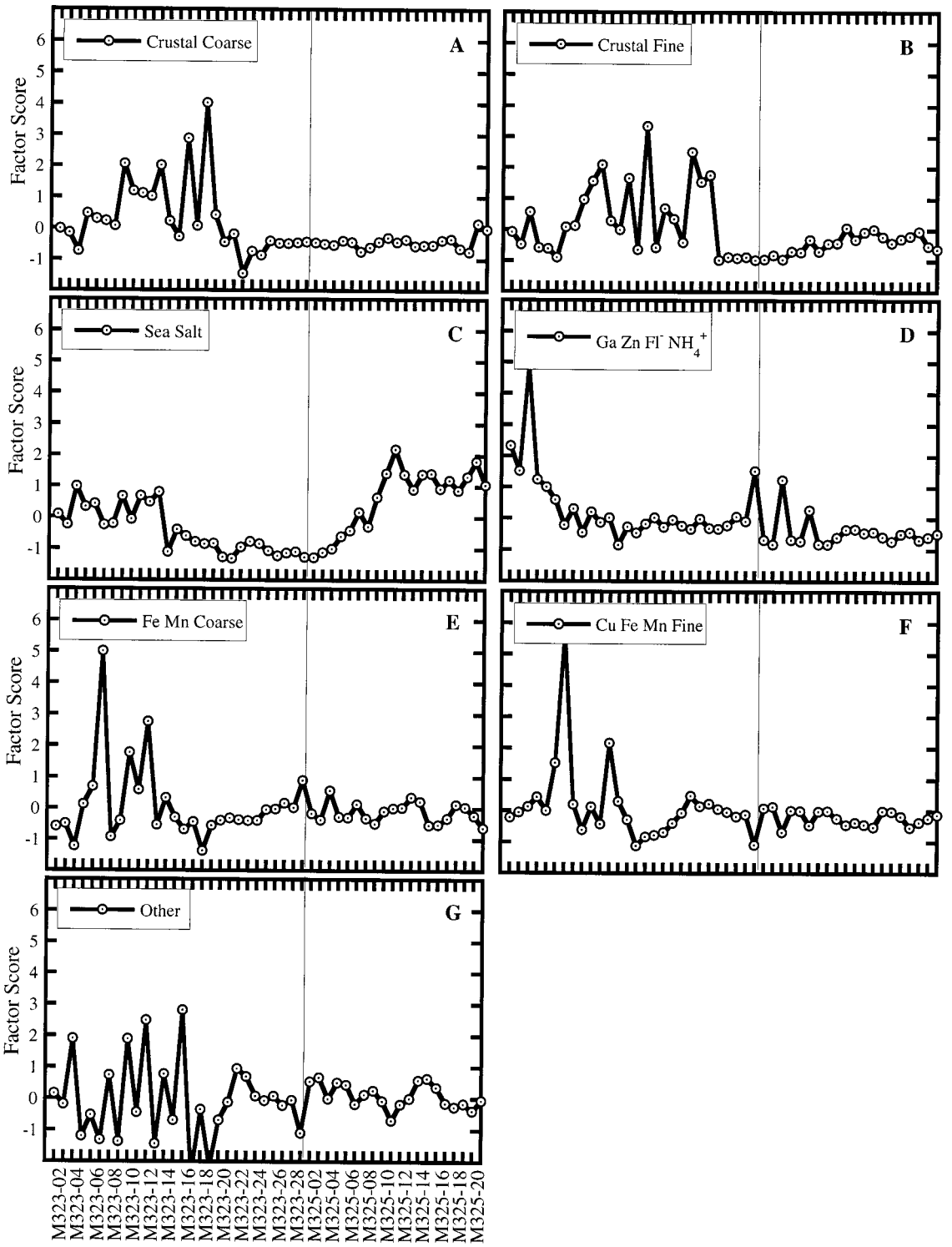

Figure 6. Factor score plots for the first seven principal components shown in Table 6.

sults indicate that $Fe(II)_{aq,labile,FINE}$ concentrations cannot be predicted from other elements (including total iron) and that other processes including atmospheric reactions are influencing the $Fe(II)_{aq,labile,FINE}$ concentrations.

4. Conclusions

Ambient aerosol samples were collected and analyzed for trace metals, anions, cations, and three labile-Fe(II) fractions during the intermonsoon and southwest monsoon periods of 1995 over the Arabian Sea aboard the German research vessel *Meteor* (*Meteor* Cruise 32). Enrichment factor and principal component analyses revealed the major sources of variances to the aerosol composition to be of crustal nature during the intermonsoon, while most of the variance during the southwest monsoon was accounted for by the sea-salt component. These findings were in agreement with the back trajectory analysis

Table 8. Sector Sampling System Operation

Sample	Time out of Sector, min	Time out of Sector, %	Ship Plume Passed Over Samplers
M323-1	0	0.0	no
M323-2	0	0.0	no
M323-3	0	0.0	no
M323-4	30	3.7	yes
M323-5	20	2.9	yes
M323-6	10	1.8	yes
M323-7	0	0.0	no
M323-8	0	0.0	no
M323-9	30	2.5	yes
M323-10	0	0.0	no
M323-11	60	7.3	yes
M323-12	10	0.7	yes
M323-13[a]			

[a]Sector sampler system now in operation (M323: ±90°, M325: ±60°).

done for both cruises. A few of the highly enriched (enriched over the crustal average) elements (e.g., Mn, Mo, Fe) were discussed in greater detail. An ultramafic crustal nature as a source of these enriched elements was not completely ruled out; however, their source could also be from an anthropogenic source or from a contamination source from the ship.

Total atmospheric aqueous-labile-Fe(II) concentrations during the intermonsoon were between 4.75 and <0.4 ng m^{-3}. In contrast, during the southwest monsoon the labile-Fe(II) concentrations were consistently below detection limit (<0.34 to <0.089 ng m^{-3}, depending on the volume of air sampled). The total labile-Fe(II) represented only a small fraction ($<4\%$) of the total Fe. The sequential extraction procedure also revealed that most of the labile-Fe(II) ($>80\%$) was released from the fine fraction (<3 μm) rather than from the coarse fraction (>3 μm). This may have important implications on the bioavailability of iron once it reaches surface waters.

Acknowledgments. Special thanks are extended to the crew of the FS *Meteor* for their help. We also thank J. J. Morgan (Caltech) and M. O. Andreae (Max Planck Institute for Chemistry, Mainz, Germany) for helpful discussions. Support for this research has been provided by a grant from the National Science Foundation, Division of Atmospheric Sciences, Atmospheric Chemistry Section (ATM 9015775; ATM 9303024). This research was also sponsored by the U.S. Department of Energy, Office of Energy Research, Environmental Sciences Division, Office of Health and Environmental Research, under appointment to the Graduate Fellowships for Global Change administered by Oak Ridge Institute for Science and Education.

References

Arimoto, R., and R. A. Duce, Dry deposition models and the air/sea exchange of trace elements, *J. Geophys. Res*., *91*, 2787–2792, 1986.

Behra, P., and L. Sigg, Evidence for redox cycling of iron in atmospheric water droplets, *Nature*, *344*, 419–421, 1990.

Berglund, J., and L. I. Elding, Manganese-catalyzed autooxidation of dissolved sulfur-dioxide in the atmospheric aqueous-phase, *Atmos. Environ*., *29*, 1379–1391, 1995.

Berglund, J., S. Fronaeus, and L. I. Elding, Kinetics and mechanism for manganese-catalyzed oxidation of sulfur(IV) by oxygen in aqueous-solution, *Inorg. Chem*., *32*, 4527–4538, 1993.

Capone, D. G., A. Subramaniam, J. P. Montoya, M. Voss, C. Humborg, A. M. Johansen, R. L. Siefert, and E. J. Carpenter, An extensive bloom of the N_2-fixing cyanobacterium *Trichodesmium erythraeum*, in the central Arabian Sea, *Mar. Ecol. Prog. Ser*., *172*, 281–292, 1998.

Carter, P., Spectrophotometric determination of serum iron at the submicrogram level with a new reagent (ferrozine), *Anal. Biochem*., *40*, 450–458, 1971.

Cass, G. R., and G. J. McRae, Source-receptor reconciliation of routine air monitoring data for trace metals: An emission inventory assisted approach, *Environ. Sci. Technol*., *17*, 129–139, 1983.

Chester, R., A. S. Berry, and K. J. T. Murphy, The distributions of particulate atmospheric trace metals and mineral aerosols over the Indian Ocean, *Mar. Chem*., *34*, 261–290, 1991.

Conklin, M. H., and M. R. Hoffmann, Metal ion-sulfur(IV) chemistry, 2, Kinetic studies of the redox chemistry of copper(II)-sulfur(IV) complexes, *Environ. Sci. Technol*., *22*, 891–898, 1988a.

Conklin, M. H., and M. R. Hoffmann, Metal ion-sulfur(IV) chemistry, 3, Thermodynamics and kinetics of transient iron(III)-sulfur(IV) complexes, *Environ. Sci. Technol*., *22*, 899–907, 1988b.

Derrick, M., and J. Moyers, Precise and sensitive water soluble ion extraction method for aerosol samples collected on polytetrafluoroethylene filters, *Anal. Lett*., *14*, 1637–1652, 1981.

Ditullio, G. R., D. A. Hutchins, and K. W. Bruland, Interaction of iron and major nutrients controls phytoplankton growth and species composition in the tropical North Pacific Ocean, *Limnol. Oceanogr*., *38*, 495–508, 1993.

Duce, R. A., G. L. Hoffman, and W. H. Zoller, Atmospheric trace metals at remote northern and southern hemisphere sites: Pollution or natural, *Science*, *187*, 59–61, 1975.

Erel, Y., S. O. Pehkonen, and M. R. Hoffmann, Redox chemistry of iron in fog and stratus clouds, *J. Geophys. Res*., *98*, 18,423–18,434, 1993.

Faure, G., *Principles and Applications of Inorganic Geochemistry*, Macmillan, Indianapolis, Ind., 1991.

Faust, B. C., and J. M. Allen, Sunlight-initiated partial inhibition of the dissolved iron(III)-catalyzed oxidation of S(IV) species by molecular-oxygen in aqueous-solution, *Atmos. Environ*., *28*, 745–748, 1994.

Faust, B. C., and M. R. Hoffmann, Photoinduced reductive dissolution of alpha-Fe_2O_3 by bisulfite, *Environ. Sci. Technol*., *20*, 943–948, 1986.

Faust, B. C., and J. Hoigné, Photolysis of Fe(III)-hydroxy complexes as sources of OH radicals in clouds, fog and rain, *Atmos. Environ*., *Part A*, *24*, 79–89, 1990.

Findlater, J., A major low-level air current near the Indian Ocean during the northern summer, *Q. J. R. Meteorol. Soc*., *95*, 362–380, 1969.

Fuzzi, S., G. Orsi, G. Nardini, M. C. Facchini, E. McLaren, and M. Mariotti, Heterogeneous processes in the Po Valley radiation fog, *J. Geophys. Res*., *93*, 11,141–11,151, 1988.

Galloway, J. N., J. D. Thornton, S. A. Norton, H. L. Volchok, and R. A. N. Mclean, Trace-metals in atmospheric deposition—A review and assessment, *Atmos. Environ*., *16*, 1677–1700, 1982.

Gomes, L., and D. A. Gillette, A comparison of characteristics of aerosol from dust storms in central Asia with soil derived dust from other regions, *Atmos. Environ*., *27*, 2539–2544, 1993.

Graedel, T. E., M. L. Mandich, and C. J. Weschler, Kinetic model studies of atmospheric droplet chemistry, 2, Homogenous transition metal chemistry in raindrops, *J. Geophys. Res*., *91*, 5205–5221, 1986.

Hess, P. C., *Origins of Igneous Rocks*, Harvard Univ. Press, Cambridge, Mass., 1989.

Hoffmann, M. R., and D. J. Jacob, Kinetics and mechanism of the catalytic oxidation of dissolved SO_2 in atmospheric droplets: Free radical, polar and photoassisted pathways, in *SO_2, NO, NO_2 Oxidation Mechanisms: Atmospheric Considerations*, edited by J. G. Calvert, pp. 101–172, Butterworth-Heinemann, Newton, Mass., 1984.

Hudson, R. J. M., and F. M. M. Morel, Iron transport in marine phytoplankton: Kinetics of cellular and medium coordination reactions, *Limnol. Oceanogr*., *35*, 1002–1020, 1990.

Hudson, R. J. M., and F. M. M. Morel, Trace-metal transport by marine microorganisms: Implications of metal coordination kinetics, *Deep Sea Res*., *40*, 129–150, 1993.

Jacob, D. J., and M. R. Hoffmann, A dynamic model for the production of H^+, NO_3^-, and SO_4^{2-} in urban fog, *J. Geophys. Res*., *88*, 6611–6621, 1983.

Jacob, D. J., J. M. Waldman, J. W. Munger, and M. R. Hoffmann, Chemical composition of fogwater collected along the California coast, *Environ. Sci. Technol*., *19*, 730–736, 1985.

Jacob, D. J., E. W. Gottlieb, and M. J. Prather, Chemistry of the polluted boundary layer, *J. Geophys. Res*., *94*, 12,975–13,002, 1989.

Kolber, Z. S., R. T. Barber, K. H. Coale, S. E. Fitzwater, R. M. Greene, K. S. Johnson, S. Lindley, and P. G. Falkowski, Iron limitation of phytoplankton photosynthesis in the equatorial Pacific Ocean, *Nature*, *371*, 145–149, 1994.

Kopcewicz, B., and M. Kopcewicz, Mossbauer study of iron-containing atmospheric aerosols, *Struct. Chem*., *2*, 303–312, 1991.

Kopcewicz, B., and M. Kopcewicz, Seasonal variations of iron concentration in atmospheric aerosols, *Hyperfine Interactions*, *71*, 1457–1460, 1992.

Kotronarou, A., and L. Sigg, SO_2 oxidation in atmospheric water: Role of Fe(II) and effect of ligands, *Environ. Sci. Technol*., *27*, 2725–2735, 1993.

Kraft, J., and R. Van Eldik, Kinetics and mechanism of the iron(III)-catalyzed autooxidation of sulfur(IV) oxides in aqueous-solution, 2, Decomposition of transient iron(III) sulfur(IV) complexes, *Inorg. Chem*., *28*, 2306–2312, 1989.

Lantzy, R. J., and F. T. Mackenzie, Atmospheric trace metals: Global cycles and assessment of man's impact, *Geochim. Cosmochim. Acta*, *43*, 511–523, 1979.

Ligocki, M. P., L. G. Salmon, T. Fall, M. C. Jone, W. W. Nazaroff, and G. R. Cass, Characteristics of airborne particles inside southern California museums, *Atmos. Environ*., *27*, 697–711, 1993.

Martin, J. H., and R. M. Gordon, Northeast Pacific iron distributions in relation to phytoplankton productivity, *Deep Sea Res*., *Part A*, *35*, 177–196, 1988.

Martin, J. H., et al., Testing the iron hypothesis in ecosystems of the equatorial Pacific Ocean, *Nature*, *371*, 123–129, 1994.

Martin, L. R., and T. W. Good, Catalyzed oxidation of sulfur dioxide in solution: The iron-manganese synergism, *Atmos. Environ*., *25*, 2395–2399, 1991.

Martin, L. R., and H. W. Hill, The iron catalyzed oxidation of sulfur: Reconciliation of the literature rates, *Atmos. Environ*., *21*, 1487–1490, 1987.

Martin, L. R., M. W. Hill, A. F. Tai, and T. W. Good, The iron-catalyzed oxidation of sulfur(IV) in aqueous-solution: Differing effects of organics at high and low *p*H, *J. Geophys. Res*., *96*, 3085–3097, 1991.

Matthijsen, J., P. J. H. Builtjes, and D. L. Sedlak, Cloud model experiments of the effect of iron and copper on tropospheric ozone under marine and continental conditions, *Meteorol. Atmos. Phys*., *57*, 43–60, 1995.

Morel, F. M. M., R. J. M. Hudson, and N. M. Price, Limitation of productivity by trace-metals in the sea, *Limnol. Oceanogr*., *36*, 1742–1745, 1991.

Munger, J. W., J. M. Waldman, D. J. Jacob, and M. R. Hoffmann, Fogwater chemistry in an urban atmosphere, *J. Geophys. Res*., *88*, 5109–5121, 1983.

Nriagu, J. O., A global assessment of natural sources of atmospheric trace metals, *Nature*, *338*, 47–49, 1989.

Nriagu, J. O., and C. I. Davidson, Toxic metals in the atmosphere, in *Advances in Environmental Science and Technology*, John Wiley, New York, 1986.

Patterson, C. C., and D. M. Settle, The reduction of orders of magnitude errors in lead analysis of biological materials and natural waters by evaluating and controlling the extent and sources of industrial lead contamination introduced during sampling, collecting, handling and analysis, *Natl. Bur. Stand. Spec. Publ*., *422*, 321–351, 1976.

Price, N. M., B. A. Ahner, and F. M. M. Morel, The equatorial Pacific Ocean—Grazer controlled phytoplankton populations in an iron limited ecosystem, *Limnol. Oceanogr*., *39*, 520–534, 1994.

Puxbaum, H., Metal compounds in the atmosphere, in *Metals and Their Compounds in the Environment*, edited by E. Merian, pp. 257–286, VCH, New York, 1991.

Rojas, C. R., R. E. Van Grieken, and R. Laane, Comparison of three dry deposition models applied to field measurements in the southern bight of the North Sea, *Atmos. Environ*., *Part A*, *27*, 363–370, 1993.

Savoie, D. L., J. M. Prospero, and R. T. Nees, Nitrate, non-sea-salt sulfate, and mineral aerosol over the northwestern Indian Ocean, *J. Geophys. Res*., *92*, 933–942, 1987.

Schlesinger, W. H., and A. E. Hartley, A global budget for atmospheric NH_3, *Biogeochemistry*, *15*, 191–211, 1992.

Schroeder, W. H., M. Dobson, D. M. Kane, and N. D. Johnson, Toxic trace elements associated with airborne particulate matter: A review, *J. Air Pollut. Control Assoc*., *37*, 1267–1285, 1987.

Sedlak, D. L., and J. Hoigné, The role of copper and oxalate in the redox cycling of iron in atmospheric waters, *Atmos. Environ*., *27*, 2173–2185, 1993.

Sedlak, D. L., and J. Hoigné, Oxidation of S(IV) in atmospheric water by photooxidants and iron in the presence of copper, *Environ. Sci. Technol*., *28*, 1898–1906, 1994.

Seigneur, C., and E. Constantinou, Chemical kinetic mechanism for atmospheric chromium, *Environ. Sci. Technol*., *29*, 222–231, 1995.

Seinfeld, J. H., *Atmospheric Chemistry and Physics of Air Pollution*, 738 pp., John Wiley, New York, 1986.

Siefert, R. L., S. O. Pehkonen, Y. Erel, and M. R. Hoffmann, Iron photochemistry of aqueous suspensions of ambient aerosol with added organic acids, *Geochim. Cosmochim. Acta*, *58*, 3271–3279, 1994.

Siefert, R. L., S. M. Webb, and M. R. Hoffmann, Determination of photochemically available iron in ambient aerosol, *J. Geophys. Res*., *101*, 14,441–14,449, 1996.

Solomon, P. A., J. L. Moyers, and R. A. Fletcher, High-volume dichotomous virtual impactor for the fractionation and collection of particles according to aerodynamic size, *Aerosol Sci. Technol*., *2*, 455–464, 1983.

Spokes, L. J., T. D. Jickells, and B. Lim, Solubilization of aerosol trace metals by cloud processing: A laboratory study, *Geochim. Cosmochim. Acta*, *58*, 3281–3287, 1994.

Stookey, L. L., Ferrozine—A new spectrophotometric reagent for iron, *Anal. Chem*., *42*, 119–781, 1970.

Taylor, S. R., and S. M. McLennan, *The Continental Crust: Its Composition and Evolution*, pp. 9–52, Blackwell Sci., Cambridge, Mass., 1985.

Turekian, K. K., and K. H. Wedepohl, Distribution of the elements in some major units of the Earth's crust, *Geol. Soc. Am. Bull*., *72*, 175–192, 1961.

Vinogradov, A. P., Average contents of chemical elements in the principal types of igneous rocks of the Earth's crust, *Geochemistry*, *7*, 641–664, 1962.

Waldman, J. M., J. W. Munger, D. J. Jacob, R. C. Flagan, J. J. Morgan, and M. R. Hoffmann, The chemical composition of acid fog, *Science*, *218*, 677–680, 1982.

Wells, M. L., N. M. Price, and K. W. Bruland, Iron limitation and the cyanobacterium synechococcus in equatorial Pacific waters, *Limnol. Oceanogr*., *39*, 1481–1486, 1994.

Wells, M. L., N. M. Price, and K. W. Bruland, Iron chemistry in seawater and its relationship to phytoplankton: A workshop report, *Mar. Chem*., *48*, 157–182, 1995.

Weschler, C. J., M. L. Mandich, and T. E. Graedel, Speciation, photosensitivity, and reactions of transition metal ions in atmospheric droplets, *J. Geophys. Res*., *91*, 5189–5204, 1986.

Xue, H. B., M. D. S. Goncalves, M. Reutlinger, L. Sigg, and W. Stumm, Copper(I) in fogwater: Determination and interactions with sulfite, *Environ. Sci. Technol*., *25*, 1716–1722, 1991.

Zhu, X. R., J. M. Prospero, D. L. Savoie, F. J. Millero, R. G. Zika, and E. S. Saltzman, Photoreduction of iron(III) in marine mineral aerosol solutions, *J. Geophys. Res*., *98*, 9039–9046, 1993.

Zhuang, G., Z. Yi, R. A. Duce, and P. R. Brown, The chemistry of iron in marine aerosols, *Global Biogeochem. Cycles*, *6*, 711, 1992a.

Zhuang, G., Z. Yi, R. A. Duce, and P. R. Brown, Link between iron and sulfur cycles suggested by detection of Fe(II) in remote marine aerosols, *Nature*, *355*, 537–539, 1992b.

Zoller, W. H., R. A. Gordon, and R. A. Duce, Atmospheric concentrations and sources of trace metals at the South Pole, *Science*, *183*, 198–200, 1974.

Zuo, Y., and J. Hoigné, Formation of hydrogen peroxide and depletion of oxalic acid in atmospheric water by photolysis of iron(III)-oxalato compounds, *Environ. Sci. Technol*., *26*, 1014–1022, 1992.

Zuo, Y. G., and J. Hoigné, Photochemical decomposition of oxalic, glyoxalic and pyruvic-acid catalyzed by iron in atmospheric waters, *Atmos. Environ*., *28*, 1231–1239, 1994.

M. R. Hoffmann (corresponding author) and A. M. Johansen, Environmental Engineering Science, W. M. Keck Laboratories, California Institute of Technology, Pasadena, CA 91125. (e-mail: mrh@cco.caltech.edu)

R. L. Siefert, Chesapeake Biological Laboratory, University of Maryland Center for Environmental Science, P.O. Box 38, One Williams Street, Solomons, MD 20688.

(Received July 2, 1998; revised October 20, 1998;
accepted October 26, 1998.)